

# Multiobjective Optimal Control Methods for Fluid Flow Using Reduced Order Modeling

Sebastian Peitz<sup>\*</sup>, Sina Ober-Blöbaum<sup>\*\*</sup>, and Michael Dellnitz<sup>\*</sup>

<sup>\*</sup>Department of Mathematics, University of Paderborn, Warburger Str. 100, D-33098 Paderborn

<sup>\*\*</sup>Department of Engineering Science, University of Oxford, Parks Road, Oxford OX1 3PJ, UK

March 16, 2022

## Abstract

In a wide range of applications it is desirable to optimally control a dynamical system with respect to concurrent, potentially competing goals. This gives rise to a multiobjective optimal control problem where, instead of computing a single optimal solution, the set of optimal compromises, the so-called Pareto set, has to be approximated. When the problem under consideration is described by a partial differential equation (PDE), as is the case for fluid flow, the computational cost rapidly increases and makes its direct treatment infeasible. Reduced order modeling is a very popular method to reduce the computational cost, in particular in a multi query context such as uncertainty quantification, parameter estimation or optimization. In this article, we show how to combine reduced order modeling and multiobjective optimal control techniques in order to efficiently solve multiobjective optimal control problems constrained by PDEs. We consider a global, derivative free optimization method as well as a local, gradient based approach for which the optimality system is derived in two different ways. The methods are compared with regard to the solution quality as well as the computational effort, and they are illustrated using the example of the two-dimensional incompressible flow around a cylinder. To the best of our knowledge, this is the first article where multiobjective optimal control is applied in the context of nonlinear PDEs.

## 1 Introduction

In many applications from industry and economy, one is interested in simultaneously optimizing several criteria. For example, in transportation one wants to reach a destination as fast as possible while minimizing the energy consumption. This example illustrates that in general, the different objectives contradict each other. Therefore, the task of computing the set of optimal compromises between the conflicting objectives, the so-called *Pareto set*, arises. This leads to a multiobjective optimization problem (MOP) or, if the control variable is a function, a multiobjective optimal control problem (MOCP). Based on the knowledge of the Pareto set, a *decision maker* can use this

---

information either for improved system design or for changing control parameters during operation as a reaction on external influences or changes in the system state itself.

Multiobjective optimization is an active area of research. Different approaches exist to address MOPs, e. g. deterministic approaches [Mie99, Ehr05], where ideas from scalar optimization theory are extended to the multiobjective situation. In many cases, the resulting solution method involves solving multiple scalar optimization problems consecutively. Continuation methods make use of the fact that under certain smoothness assumptions the Pareto set is a manifold that can be approximated by continuation methods known from dynamical systems theory [Hil01]. Another prominent approach is based on evolutionary algorithms [AJG05, Deb99, ZDT00], where the underlying idea is to evolve an entire set of solutions (population) during the optimization process. Set oriented methods provide an alternative deterministic approach to the solution of MOPs. Utilizing subdivision techniques, the desired Pareto set is approximated by a nested sequence of increasingly refined box coverings [DSH05, SWOBD13].

When dealing with control functions, a multiobjective optimal control problem (MOCP) needs to be solved. Similar to MOPs, ideas from scalar optimal control theory can be extended to take into account multiple objectives. By applying a direct method [HPUU08], the MOCP is transformed into a high-dimensional, nonlinear MOP such that the methods mentioned before can be applied. Another approach is based on the transformation of the MOCP into a sequence of scalar optimal control problems and the use of well established optimal control techniques for their solution. Examples for MOCPs can be found e. g. in [DEF<sup>+</sup>14, LHDVI10, OBRzF12, SWOBD13] with ODE constraints. In [LKBM05], nonlinear PDE constraints are taken into account but the model is treated as a black box, i. e. no special treatment of the constraints is required. Fluid flow applications have been considered in [OBPG15, PD15].

All approaches to MOP / MOCP have in common that a large number of function evaluations is typically required. Thus, the direct computation of the Pareto set can quickly become numerically infeasible. This is frequently the case for problems described by (nonlinear) partial differential equations such as the Navier-Stokes equations for fluid flow. Standard optimization methods for PDEs [HPUU08] often make use of a discretization by finite elements, finite volumes or finite differences which results in a high-dimensional system of ODEs. In a multi query context (such as optimization, parameter identification, etc.), this approach often exceeds the limits of today's computing power. Hence, one aims for methods which reduce the computational cost significantly. This can be achieved by approximating the PDE by a reduced order model of low dimension.

In recent years, major achievements were made in the field of reduced order modeling [SvdVR05, BMS05]. In fact, different methods for creating low dimensional models exist for linear systems (e. g. [WP02]) as well as for nonlinear systems (e. g. [BMNP04, GMNP07]), see [ASG01] for a survey. Many researchers focus their attention to the Navier-Stokes equations (e. g. [CBS05, Row05, XFB<sup>+</sup>14]), where *Proper Orthogonal Decomposition* (POD) [HLB98] has proven to be a powerful tool. In the context of fluids, this technique has first been introduced by Lumley [Lum67] to identify coherent structures. Reduced order models using POD modes and the *method of snapshots* go back to Sirovich [Sir87].

Due to the wide spectrum of potential applications (optimal mixing, drag reduction, HVAC, etc.) and the progress in computational capabilities, a lot of research is devoted to the control of the Navier-Stokes equations, either directly [GeH89, Lac14] or via reduced order modeling [GPT99,

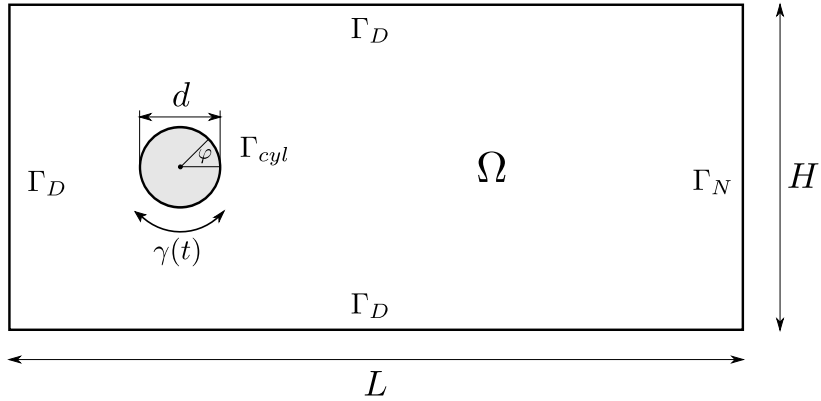


**Figure 1:** Sketch of the domain  $\Omega \subset \mathbb{R}^2$ .

[Fah00, IR01, BCB05, BCB07, PD15]. In many cases, the energy consumption plays an important role. Thus, ideally, one wants to consider the control cost in addition to the main objective in order to choose a good trade-off between the achievement of the desired objective and the respective control cost. Since this causes a considerable computational effort in case of systems described by the Navier-Stokes equations, we show in this article how reduced order modeling and multiobjective optimal control methods can be combined to solve MOCPs with nonlinear PDE constraints. Using model order reduction via POD and Galerkin projection, we present several methods to compute the Pareto set for the conflicting objectives *minimization of flow field fluctuations* and *control cost* for the two-dimensional flow around a cylinder at  $Re = 200$ . We discuss the advantages and disadvantages of the different approaches and comment on the respective computational cost. In fact, it is shown that the different methods strongly differ in their respective efficiency and that a thorough mathematical derivation of the optimality system yields a considerably improved performance. We also show that the choice of the algorithm and the corresponding particular numerical realization of the cost functional lead to different optimal control behavior.

The article is organized as follows. In Section 2 we present the problem setting and formulate the MOCP. After an introduction to multiobjective optimal control in Section 3, the reduced order model and the resulting reduced MOCP are derived in Section 4. We then present our results in Section 5 and draw a conclusion in Section 6.

## 2 Problem formulation

The two-dimensional, viscous flow around a cylinder is one of the most extensively studied cases for separated flows in general as well as for flow control problems [GPT99, GBZI04, BCB05]. In this paper, we consider the laminar case described by the incompressible Navier-Stokes equations at a Reynolds Number  $Re = \frac{U_\infty d}{\nu} = 200$  computed with respect to the far field velocity  $U_\infty$ , the

---

kinematic viscosity  $\nu$  and the cylinder diameter  $d$ :

$$\frac{\partial U(x, t)}{\partial t} + (U(x, t) \cdot \nabla) U(x, t) = -\frac{\nabla p(x, t)}{\rho} + \frac{1}{Re} \nabla^2 U(x, t), \quad (1a)$$

$$\nabla \cdot U(x, t) = 0, \quad (1b)$$

$$(U(x, 0), p(x, 0)) = (U_0(x), p_0(x)), \quad (1c)$$

$$\text{for } x \in \Omega, t \in [t_0, t_e],$$

where  $U \in H^2(\Omega \times [t_0, t_e], \mathbb{R}^2)$  is the two-dimensional fluid velocity and  $p \in H^1(\Omega \times [t_0, t_e], \mathbb{R})$  the pressure.  $H^k$  is the Sobolev space  $W^{k,2}$  equipped with the inner product  $(u, v)_{W^{k,2}} = \sum_{i=0}^k \int_{\Omega} D^i u(x) \cdot D^i v(x) dx$  and the respective norm  $\|u\|_{W^{k,2}} = \left( \sum_{i=0}^k \int_{\Omega} D^i u(x) \cdot D^i u(x) dx \right)^{1/2}$  [HPUU08]. The domain (Figure 1) is denoted by  $\Omega$ . We impose Dirichlet boundary conditions at the inflow as well as the upper and lower walls  $\Gamma_D$ . At the outflow  $\Gamma_N$ , we impose a standard *no shear stress* condition [HRT96]:

$$U(x, t) = (U_{\infty}, 0) \quad \text{for } x \in \Gamma_D, \quad (1d)$$

$$p(x, t) \mathbf{n} = \frac{1}{Re} \frac{\partial U(x, t)}{\partial \mathbf{n}} \quad \text{for } x \in \Gamma_N, \quad (1e)$$

where  $\mathbf{n} \in \mathbb{R}^2$  is the vector normal to the boundary. On the cylinder  $\Gamma_{cyl}$ , we prescribe a time-dependent Dirichlet BC such that it performs a rotation around its center with the angular velocity  $\gamma(t)$ :

$$U(x, t) = \frac{d}{2} \gamma(t) \begin{pmatrix} -\sin(\varphi) \\ \cos(\varphi) \end{pmatrix} \quad \text{for } x \in \Gamma_{cyl}, \quad (1f)$$

with  $\varphi$  according to Figure 1. The cylinder rotation  $\gamma(t) \in L^2([t_0, t_e], \mathbb{R})$  serves as the control mechanism for the flow. The Hilbert space  $L^2$  is equipped with the inner product  $(u, v)_{L^2} = \int_{t_0}^{t_e} u(t) \cdot v(t) dt$  and the norm  $\|u\|_{L^2} = \left( \int_{t_0}^{t_e} u(t) \cdot u(t) dt \right)^{1/2}$ .

Following [Fah00, BCB05], we introduce the weak formulation of (1a). Consider the divergence free Hilbert space of test functions  $V = \{\phi \in H^1(\Omega \times [t_0, t_e], \mathbb{R}^2) \mid \nabla \cdot \phi = 0\}$ . Then, a function  $U \in H^1(\Omega \times [t_0, t_e], \mathbb{R}^2)$  which satisfies

$$\left( \frac{\partial U}{\partial t} + (U \cdot \nabla) U, \phi \right) = \left( \frac{p}{\rho}, \nabla \cdot \phi \right) - [p\phi] - \frac{1}{Re} (\nabla \phi, (\nabla U)^T) + \frac{1}{Re} [(\nabla U)^T \phi] \quad (2)$$

for all  $\phi \in V$  is called a *weak solution* of (1a). Here,  $(A, B) = \sum_{i,j} \int_{\Omega} A_{i,j} B_{i,j} dx$  and  $[U] = \int_{\Gamma} U(x) \cdot \mathbf{n} dx$ . Note that (1b) is automatically satisfied by design of the test function space  $V$ .

## 2.1 Finite volume discretization

The system (1a – 1f) is solved by the software package *OpenFOAM* [JJT07] using a finite volume discretization and the *PISO* scheme [FP12]. We have chosen *OpenFOAM* because it contains a

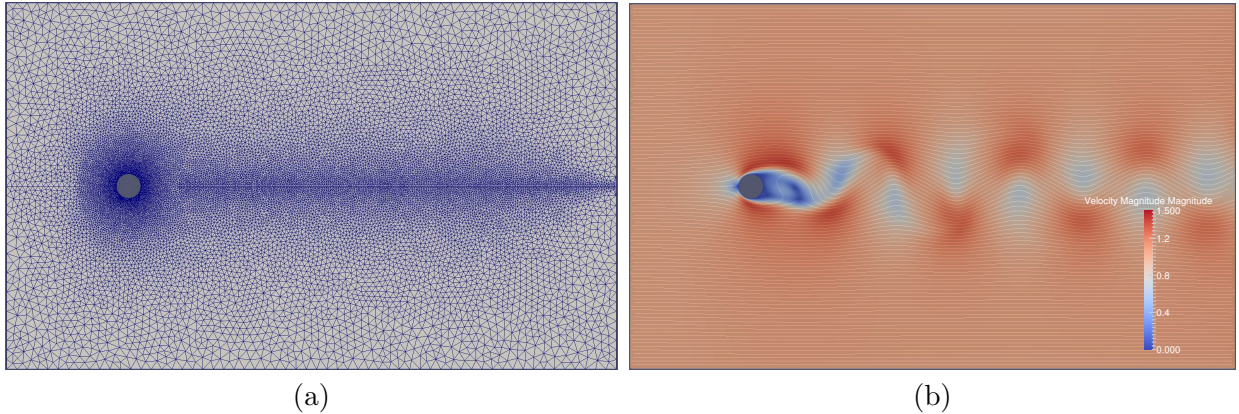


**Figure 2:** (a) FEM discretization of the domain  $\Omega$  by a triangular mesh ( $n = 17.048$ ). (b) Solution for  $\gamma(t) = 0$ : *von Kármán vortex street*.

variety of efficient solvers for fluid flow applications that can be used for many applications. Since the theory as well as the computation of the reduced order model utilize finite elements, we then, in the spirit of data driven modeling, map our solution to a finite element mesh with  $n = 17.048$  degrees of freedom (Figure 2(a)). Finally, the velocity field can be written in terms of the FEM basis:

$$U(x, t) = \begin{pmatrix} \sum_{i=1}^n \mathbf{U}_i(t) \phi_i(x) \\ \sum_{i=1}^n \mathbf{U}_{n+i}(t) \phi_i(x) \end{pmatrix}, \quad (2.3)$$

where  $\mathbf{U}(t) \in \mathbb{R}^{2n}$  are the nodal values of the two velocity components and  $\{\phi_i(x)\}_{i=1}^n$  are the FEM basis functions. All finite element related computations are performed with the *FEniCS* toolbox [LMW12] using linear basis functions.

For a non-rotating cylinder, i. e.  $\gamma(t) = 0$ , the system possesses a periodic solution, the well-known *von Kármán vortex street* (Figure 2(b)), where vortices separate alternately from the upper and lower surface of the cylinder, respectively. The effect is observed frequently in nature and is one of the most studied phenomena in fluid mechanics, also in the context of flow control, where the objective is to stabilize the flow and to reduce the drag.

## 2.2 Multiobjective optimal control problem

In many applications, the control cost is of great interest. This is immediately clear when the goal of the optimization is to save energy such that in this case, the control effort needs to be taken into account. In scalar optimization problems, this is often done by adding an additional term of the form  $\beta \int_{t_0}^{t_e} \gamma(t) dt$  to the cost functional where  $\beta \in \mathbb{R}_{\geq 0}$  is a weighting parameter. Here, we want to consider the two objectives flow stabilization, i. e. the minimization of the fluctuations  $u(x, t) = U(x, t) - \langle U(x) \rangle$  around the mean flow field  $\langle U(x) \rangle = \frac{1}{T} \int_0^T U(x, t) dt$ , and the minimization

---

of the control cost separately which leads to the following multiobjective optimal control problem:

$$\min_{U, \gamma} \widehat{J}(U, \gamma) = \min_{U, \gamma} \left( \begin{array}{c} \int_{t_0}^{t_e} \|u(\cdot, t)\|_{L^2}^2 dt \\ \|\gamma\|_{L^2}^2 \end{array} \right),$$

where  $\widehat{J} : H^2(\Omega \times [t_0, t_e], \mathbb{R}^2) \times L^2([t_0, t_e], \mathbb{R}) \rightarrow \mathbb{R}^2$  and  $U(x, t)$  satisfies (1a – 1f). As shown in [FGH98], there exists a unique solution  $U(x, t)$  for each  $\gamma(t)$ . Hence, from now on we denote by  $u(\gamma)$  the solution  $u(x, t)$  for a fixed  $\gamma \in L^2([t_0, t_e], \mathbb{R})$  and consider the reduced cost functional  $J : L^2([t_0, t_e], \mathbb{R}) \rightarrow \mathbb{R}^2$  which leads to the following multiobjective optimal control problem:

$$\min_{\gamma} J(\gamma) = \min_{\gamma} \left( \begin{array}{c} \int_{t_0}^{t_e} \|u\|_{L^2}^2 dt \\ \|\gamma\|_{L^2}^2 \end{array} \right). \quad (\text{MOCP})$$

In general, the solution to this problem does not consist of isolated points but a set of *optimal compromises* between the two objectives. In the following section, we give a short introduction to multiobjective optimal control theory and solution methods.

### 3 Multiobjective Optimal Control

Consider the general multiobjective optimal control problem:

$$\min_{\gamma} J(\gamma) = \min_{\gamma} \left( \begin{array}{c} J_1(\gamma) \\ \vdots \\ J_k(\gamma) \end{array} \right), \quad (3)$$

with  $J : L^2([t_0, t_e], \mathbb{R}) \rightarrow \mathbb{R}^k$  and  $J_i : L^2([t_0, t_e], \mathbb{R}) \rightarrow \mathbb{R}$ ,  $i = 1, \dots, k$ . The space in which the control functions live is denoted as the *decision space* and the function  $J$  is a mapping to the  $k$ -dimensional *objective space*. The set of feasible functions  $\gamma$  is the *feasible set in decision space*. We denote its image as the *feasible set in objective space* which consists of the *feasible points*  $J(\gamma)$ . In contrast to single objective optimization problems, there exists no total order of the objective function values in  $\mathbb{R}^k$ ,  $k \geq 2$ . Therefore, the comparison of values is defined in the following way [Mie99]:

**Definition 3.1.** Let  $v, w \in \mathbb{R}^k$ . The vector  $v$  is less than  $w$  ( $v <_p w$ ), if  $v_i < w_i$  for all  $i \in \{1, \dots, k\}$ . The relation  $\leq_p$  is defined in an analogous way.

A consequence of the lack of a total order is that we cannot expect to find isolated optimal points. Instead, the solution to (3) is the set of optimal compromises, the so-called *Pareto set* named after Vilfredo Pareto:

**Definition 3.2.**

(a) A function  $\gamma^*$  dominates a function  $\gamma$ , if  $J(\gamma^*) \leq_p J(\gamma)$  and  $J(\gamma^*) \neq J(\gamma)$ .

---

(b) A feasible function  $\gamma^*$  is called (globally) Pareto optimal if there exists no feasible function  $\gamma$  dominating  $\gamma^*$ . The image  $J(\gamma^*)$  of a (globally) Pareto optimal function  $\gamma^*$  is a (globally) Pareto optimal point.

(c) The set of nondominated feasible functions is called the Pareto set, its image the Pareto front.

Consequently, for each function that is contained in the Pareto set, one can only improve one objective by accepting a trade-off in at least one other objective. Figuratively speaking, in a two-dimensional problem, we are interested in finding the "lower left" boundary of the feasible set in objective space (cf. Figure 3(b)). More detailed introductions to multiobjective optimization can be found in [Mie99, Ehr05].

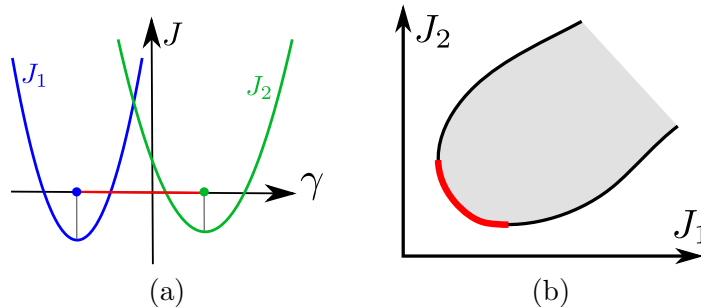


**Figure 3:** Pareto set (a) and front (b) of the multiobjective optimization problem  $\min_{\gamma \in \mathbb{R}} J(\gamma)$ ,  $J : \mathbb{R} \rightarrow \mathbb{R}^2$ .

### 3.1 Solution methods

Various methods exist to solve problem (3). In this work, we present two approaches that are fundamentally different. The first one is a reference point method [RBW<sup>+</sup>09] for which the distance between a feasible point (i. e. an objective value that lies in the feasible set in objective space) and an infeasible target in objective space is minimized. The method yields a moderate number of single objective optimization problems that are solved consecutively. The second approach is a global, derivative free subdivision algorithm [DSH05] for which the Pareto set is approximated by a nested sequence of increasingly refined box coverings. However, its applicability depends critically on both the decision space dimension and the numerical effort of function evaluations.

#### 3.1.1 Reference point method

The reference point method presented here belongs to the category of scalarization techniques for which the solution set of (3) is approximated by a finite set of points, each computed by solving a scalar optimization problem. First, a so-called *target*  $T_1 \in \mathbb{R}^k$  is chosen such that it lies outside of the feasible set in objective space. We then solve the scalar optimization problem  $\min_{\gamma_1} \|T_1 - J(\gamma_1)\|_2^2$ . As a result, the corresponding optimal point  $J(\gamma_1)$  lies on the boundary of the feasible set and it is not possible to further improve all objectives at the same time. Thus,

---

the point is Pareto optimal. By adjusting the target position, multiple points on the Pareto front (i. e.  $J(\gamma_2), J(\gamma_3), \dots$ ) are computed recursively. For  $J$  being continuous [Hil01], the change in decision space is small when the target position changes only slightly and hence, the current solution is a good initial guess for the next scalar problem which accelerates the convergence considerably.

Theoretically, the method is not restricted to low objective space dimensions. However, setting the targets properly to get an adequate and fast approximation of the Pareto front becomes complicated in higher dimensions. In our case, we are dealing with two objectives where the targets can be determined easily using linear extrapolation (cf. Figure 4 and Algorithm 1) as proposed in [RBW<sup>+</sup>09]. This also allows us to compute the whole front in at most two runs of the algorithm. From the initial point, we first proceed in one direction, e. g. decreasing  $J_1$ . When, at some point,  $J_1$  is increasing again, we know that we have reached the extremal point of the feasible set (cf. Figure 3) and the scalar optimum of  $J_1$ . We then return to the initial point and proceed in the opposite direction until the other extremal point is reached.

---

**Algorithm 1** (Reference point method for  $J \in \mathbb{R}^2$ )

---

**Require:** Target point  $T_1$ , step length parameters  $h_y, h_p$  and  $h_x$ , maximal number of points  $n_{max}$

```

1: Solve initial scalar optimization problem, e. g.  $\min_{\gamma_0} \delta J_1 + (1 - \delta)J_2, \delta \in [0, 1]$ 
2: for  $s = 1, 2$  do
3:   for  $i = 1, \dots, n_{max}/2$  do
4:     Solve scalar optimization problem  $\min_{\gamma_i} \|T_i - J(\gamma_i)\|_2^2$ 
5:     if  $J_s(\gamma_i) > J_s(\gamma_{i-1})$  (i. e. the end of the Pareto front is reached) then
6:       Redefine target  $T_1$  such that the second loop ( $s = 2$ ) proceeds into the other direction
7:       break
8:     end if
9:     Compute target  $T_{i+1} = J(\gamma_i) + h_y \frac{J(\gamma_i) - J(\gamma_{i-1})}{\|J(\gamma_i) - J(\gamma_{i-1})\|_2} + h_p \frac{T_i - J(\gamma_i)}{\|T_i - J(\gamma_i)\|_2}$ 
10:    Perform predictor step  $\gamma_{p,i+1} = \gamma_i + h_x (\gamma_i - \gamma_{i-1})$ 
11:  end for
12: end for

```

---

The scalar optimization problems can be solved using any suitable method. Here, we use backtracking as described in [NW06] and compute the derivatives using an adjoint approach. Note that since the scalar optimization routine often is of local nature, the method overall is also local and depends on the initial guesses as well as the choice of the target points. However, under certain smoothness assumptions, the Pareto set is a  $(k - 1)$ -dimensional manifold [Hil01] such that once the first point is computed correctly, the method is promising to find the globally optimal Pareto set for many problems.

**Remark 3.3.** *For the reference point method, it turned out to be numerically beneficial if  $(T_i - J_i)/(T_j - J_j) = \mathcal{O}(1) \forall i, j \in \{1, \dots, k\}$ . Otherwise, the computation of new target points may become sensitive to the step length parameters.*



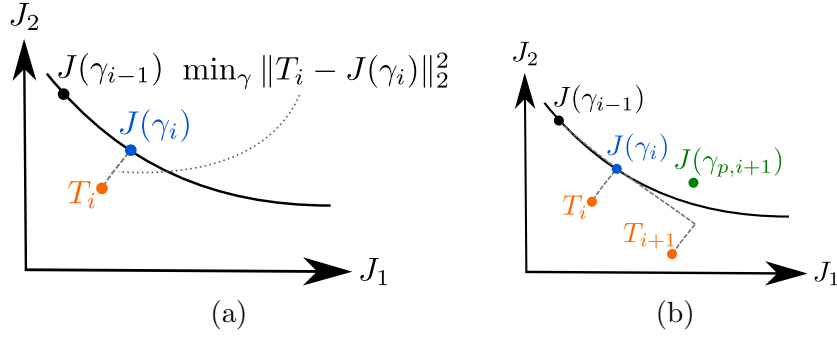


**Figure 4:** Reference point method in image space. (a) Determination of the  $i$ -th point on the Pareto front by solving a scalar optimization problem. (b) Computation of new target point  $T_{i+1}$  and predictor step in decision space  $(\gamma_{p,i+1})$ .

### 3.1.2 Global subdivision algorithm

When the image space dimension increases or, alternatively, the Pareto front is disconnected (e. g. [DEF<sup>+</sup>14]), continuation methods like the reference point method may fail. Moreover, the resulting scalar optimization problems are often solved by algorithms of local nature which may also not be sufficient if global optima are desired. The subdivision algorithm presented here overcomes these problems. It is described in more detail in [DSH05] including a proof of convergence. The version using gradient information is based on concepts for the computation of attractors of dynamical systems [DH97], it is however not considered here. Instead, we focus on the derivative free approach.

Since its applicability depends critically on both the decision space dimension and the numerical effort of function evaluations, the subdivision algorithm is limited to low decision space dimensions. Therefore, we introduce a sinusoidal control, i. e.  $\gamma(t) = A \sin(2\pi\omega t + \tau)$ . The choice is motivated by the fact that the uncontrolled dynamics of the problem at hand are also periodic. This way, we transform (MOCP) into an MOP with  $\tilde{J} : \mathbb{R}^3 \rightarrow \mathbb{R}^2$ :

$$\min_{A,\omega,\tau \in \mathbb{R}} \tilde{J}(A,\omega,\tau) = \min_{A,\omega,\tau \in \mathbb{R}} \left( \begin{array}{c} \int_{t_0}^{t_e} \|u\|_{L^2}^2 dt \\ \int_{t_0}^{t_e} (A \sin(2\pi\omega t + \tau))^2 dt \end{array} \right). \quad (\text{MOP-3D})$$

The subdivision algorithm (cf. Algorithm 2) is a set oriented method where the Pareto set is approximated by a nested sequence of increasingly refined box coverings (cf. Figure 5). During the algorithm, a sequence of box collections  $\{\mathcal{B}_i\}_{i=0,\dots}$  covering the Pareto set is constructed, starting with a sufficiently large initial set  $\mathcal{B}_0 \subset \mathbb{R}^m$ . In each iteration, the algorithm performs the steps *subdivision* and *selection* until a given precision criterion is satisfied. This way, a subset of the previous box collection remains that is a closer covering of the desired set. In the selection step, a nondominance test is performed, eliminating all boxes that are dominated by another box. Numerically, this is realized by a representative set of sampling points in each box (cf. Figure 5(a)).

---

**Algorithm 2** (Global, derivative free subdivision algorithm)

---

**Require:** Box constraints  $\gamma^{min}, \gamma^{max} \in \mathbb{R}^n$

- 1: Create initial box collection  $\mathcal{B}_0$  defined by the constraints  $\gamma^{min}, \gamma^{max}$ , i. e.  $\bigcup_{B \in \mathcal{B}_0} B = [\gamma_1^{min}, \gamma_1^{max}] \times \dots \times [\gamma_n^{min}, \gamma_n^{max}]$
  - 2: **for**  $i = 1, \dots, N$  **do**
  - 3: Subdivision step:  $\bigcup_{B \in \hat{\mathcal{B}}_i} B = \bigcup_{B \in \mathcal{B}_{i-1}} B$  such that  $\max(\text{diam}(\hat{\mathcal{B}}_i)) < \Theta \max(\text{diam}(\mathcal{B}_{i-1}))$ ,  $\Theta \in (0, 1)$
  - 4: Insert  $S$  sampling points into each box and evaluate the cost functional  $J(\gamma_s), s = 1, \dots, S$
  - 5: Selection step: Eliminate all boxes that contain only dominated points:  $\mathcal{B}_i = \left\{ B \in \hat{\mathcal{B}}_i \mid \text{There exists no } \gamma^* \in \bigcup_{\hat{B} \in \hat{\mathcal{B}}_i} \hat{B} \text{ such that } J(\gamma^*) \leq_p J(\gamma) \forall \gamma \in B \right\}$
  - 6: **end for**
- 

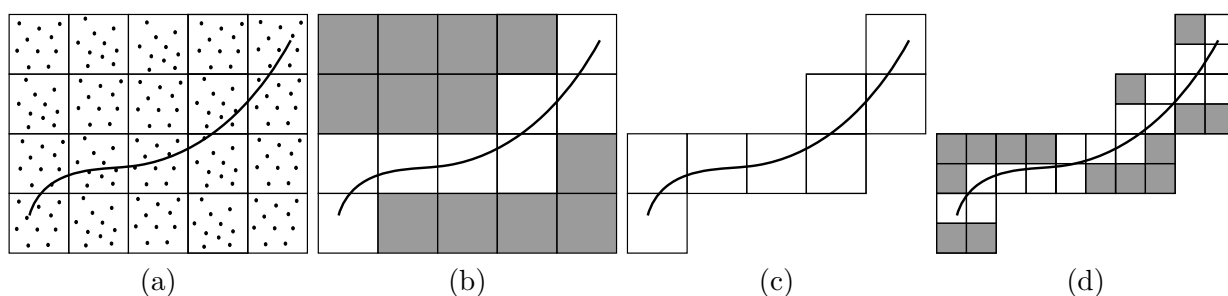


**Figure 5:** Global subdivision algorithm. (a) Sampling. (b) Nondominance test. (c) Elimination of dominated boxes. (d) Subdivision, sampling and nondominance test.

## 4 Reduced Order Modeling

The problem (MOCP) could now be solved using either of the methods presented in Section 3.1. However, both require a large number of evaluations of the cost functional and, consequently, evaluations of the system (1a – 1f). A finite element discretization yields a large number of degrees of freedom such that solving (MOCP) quickly becomes computationally infeasible. Hence, we need to reduce the cost for solving the dynamical system significantly. This is achieved by means of reduced order modeling where we replace the state equation by a reduced order model of coupled, nonlinear ordinary differential equations that can be solved much faster.

### 4.1 Reduced Order Model

The standard procedure for deriving a reduced order model is by introducing a Galerkin ansatz [HLB98]:

$$U(x, t) = \sum_{j=1}^l \alpha_j(t) \psi_j(x), \quad (x, t) \in \Omega \times [t_0, t_e], \quad (4)$$

---

where  $\alpha(t)$  are time-dependent coefficients and  $\psi_j(x) = \sum_{i=1}^n \Psi_{ji} \phi_i(x)$  are basis functions defined on the finite element space with the nodal values  $\Psi_{ji} \in \mathbb{R}^{2n}$  and FEM basis functions  $\{\phi_i\}_{i=1}^n$  (cf. (2.3)). The basis functions inherit properties from the velocity  $U$  [BHL93]. Hence, the mass conservation equation (1b) is automatically satisfied. Inserting (4) into the weak formulation of the Navier-Stokes equations (2) yields a system of  $l$  ordinary differential equations of the form

$$\dot{\alpha}(t) = \tilde{\mathcal{B}}\alpha(t) + \tilde{\mathcal{C}}(\alpha(t)),$$

where the coefficient matrices are computed by evaluating the  $L^2$  inner products:

$$\begin{aligned} \left(\tilde{\mathcal{B}}\right)_{ij} &= \frac{1}{Re} (\nabla\psi_i, \nabla\psi_j)_{L^2}, \\ \left(\tilde{\mathcal{C}}(\alpha(t))\right)_j &= \alpha(t)^T \mathcal{Q}_j \alpha(t), \\ \text{with } (\mathcal{Q}_j)_{ik} &= ((\psi_i \cdot \nabla)\psi_k, \psi_j)_{L^2}. \end{aligned}$$

This model, however, is not controllable. Moreover, it is known [Sir87] that the basis functions need to be computed from data with homogeneous boundary conditions ( $U(x, t) = 0$  for  $x \in \Gamma$ ). This way, the basis functions  $\psi_j(x)$  as well as their linear combinations also possess homogeneous boundary conditions. For these reasons, we introduce an ansatz for a flow field decomposition [Rav99, BCB05]:

$$U(x, t) = \langle U(x, t) \rangle + \gamma(t)U_c(x) + u(x, t), \quad (5)$$

where  $U_c(x)$  is a so-called *control function* which is a solution to (1a), (1b), (1c) with a constant cylinder rotation and zero boundary conditions elsewhere. The decomposition is computed in two steps:

$$\begin{aligned} U^*(x, t) &= U(x, t)|_{\gamma(t)=\gamma_{ref}(t)} - \gamma_{ref}(t)U_c(x), \\ u(x, t) &= U^*(x, t) - \langle U^*(x, t) \rangle. \end{aligned}$$

In this way,  $u(x, t) = \sum_{j=1}^l \alpha_j(t)\psi_j(x)$  satisfies homogenous boundary conditions for all  $t \in [t_0, t_e]$ . (Note that this does not hold exactly on  $\Gamma_N$ , however, the resulting error is small and hence neglected [BCB05].) Inserting (5) into (2) yields an extended reduced order model:

$$\dot{\alpha}(t) = \mathcal{A} + \mathcal{B}\alpha(t) + \mathcal{C}(\alpha(t)) + \mathcal{D}\dot{\gamma}(t) + (\mathcal{E} + \mathcal{F}\alpha(t))\gamma(t) + \mathcal{G}\gamma^2(t), \quad (6)$$

$$\alpha_j(t_0) = (u(\cdot, t_0), \psi_j)_{L^2} =: \alpha_{0,j}, \quad (7)$$

where  $\alpha \in H^1([t_0, t_e], \mathbb{R}^l)$ . The coefficient matrices  $\mathcal{A}$  to  $\mathcal{G}$  can be found in [BCB05], their size depends on the dimension  $l$  of the ROM:  $\mathcal{A}, \mathcal{D}, \mathcal{E}, \mathcal{G} \in \mathbb{R}^l$ ;  $\mathcal{B}, \mathcal{F} \in \mathbb{R}^{l,l}$ ;  $(\mathcal{C}(\alpha(t)))_j = \alpha(t)^T \mathcal{Q}_j \alpha(t)$  with  $(\mathcal{Q}_j)_{ik} = ((\psi_i \cdot \nabla)\psi_k, \psi_j)_{L^2} \in \mathbb{R}^{l,l}$ .

**Remark 4.1.** *Since the time derivative of the control occurs in (6), we require higher regularity, i. e.  $\gamma \in H^1([t_0, t_e], \mathbb{R})$ .*

---

Due to the truncation of the POD basis, the higher modes covering the small scale dynamics, i. e. the dynamics responsible for dissipation, are neglected. It is well known that this can lead to incorrect long term behavior and hence, the model needs to be modified to account for this fact and several methods were proposed to address this issue, e. g. [Rem00, SK04, NPM05, CEF09, BBI09]. Here, we achieve stabilization of the model (6) by solving an augmented optimization problem [GBZI04]. The resulting initial value problem can now be solved using a standard Runge-Kutta method.

## 4.2 Reduced order multiobjective optimal control problem

For the reduced MOCP, we replace the objectives in (MOCP) by their equivalents in the reduced order model. Since the reference point method is more stable for objectives of the same order of magnitude (cf. Remark 3.3), we additionally multiply the second component by  $l$  (i. e. the number of basis functions)

$$\min_{\alpha, \gamma} \left( \begin{array}{c} \int_{t_0}^{t_e} \int_{\Omega} \left\| \sum_{i=1}^l \alpha_i(t) \psi_i(x) \right\|_2^2 dx dt \\ l \int_{t_0}^{t_e} \gamma^2(t) dt \end{array} \right). \quad (8)$$

## 4.3 Proper orthogonal decomposition (POD)

The basis functions for the extended Galerkin ansatz (5) are computed from FEM data using the well known POD method for which the orthonormal basis  $\{\psi_i(x)\}_{i=1}^l$  is computed which is on average most similar to a set of flow field realizations  $\{u(x, t_0), \dots, u(x, t_{m-1})\}$  [Sir87]:

$$\max \sum_{j=1}^{m-1} \sum_{i=1}^l (u_j(\cdot, t_j), \psi_i)_{L^2}^2 \quad \text{s.t.} \quad (\psi_i, \psi_j)_{L^2} = \delta_{i,j}.$$

The solution to this maximization problem can be obtained by solving the following eigenvalue problem [KV02, Fah00]:

$$S^T M S v_i = \lambda_i v_i, \quad i = 1, \dots, m, \quad (9)$$

where  $S \in \mathbb{R}^{2n, m}$ ,  $S = [\mathbf{u}(t_1), \dots, \mathbf{u}(t_m)]$  is the so-called *snapshot matrix* and  $M \in \mathbb{R}^{2n, 2n}$  is the finite element mass matrix. Using the eigenvalues and eigenvectors from (9), the POD modes can be computed by again making use of the FEM basis functions  $\{\phi_i(x)\}_{i=1}^n$ :

$$\begin{aligned} \Psi_i &= \frac{1}{\sqrt{\lambda_i}} S v_i, \\ \psi_i(x) &= \sum_{j=1}^n \Psi_{ij} \phi_j(x). \end{aligned}$$

Making use of the orthonormality of the POD basis, the first objective in (8) can be simplified:

$$\begin{aligned} \int_{\Omega} \left\| \sum_{i=1}^l \alpha_i(t) \psi_i(x) \right\|_2^2 dx &= \int_{\Omega} \left( \sum_{i=1}^l \alpha_i(t) \psi_i(x) \right) \cdot \left( \sum_{i=1}^l \alpha_i(t) \psi_i(x) \right) dx = \sum_{i=1}^l \alpha_i^2(t) \\ &\text{with } (\psi_i, \psi_j)_{L^2} = \delta_{i,j}, \end{aligned}$$

which allows us to replace (8) by a simpler formulation:

$$\min_{\alpha, \gamma} \left( \begin{array}{c} \int_{t_0}^{t_e} \sum_{i=1}^l \alpha_i^2(t) dt \\ l \int_{t_0}^{t_e} \gamma^2(t) dt \end{array} \right). \quad (\text{R-MOCP})$$

The eigenvalues  $\lambda$  are a measure for the information contained in the respective modes and hence, the error between the Galerkin ansatz and the snapshot data is determined by the fraction of the truncated eigenvalues [Sir87], i. e.  $\epsilon(l) = \sum_{j=1}^l \lambda_j / \sum_{j=1}^{\infty} \lambda_j$ . By choosing a value for  $\epsilon$ , typically 0.99 or 0.999, the basis size can be determined. For many applications, the eigenvalues decay fast such that a truncation to a small basis is possible. The error  $\epsilon$  is only known for the reference control at which the data was collected. If one allows for multiple evaluations of the finite element solution, the reduced model can be updated when necessary. This is realized using trust region approaches [Fah00, BCB07]. An alternative approach is to use a reference control that yields sufficiently rich dynamics such that the model can be expected to hold for a larger variety of controls [BCB05]. Here, we follow the second approach and take 1200 snapshots in the interval  $[0, 60]$  with  $\Delta t = 0.05$  for a *chirping* reference control (cf. Figure 6). This leads to a basis of size  $l = 38$  for  $\epsilon(l) \geq 99\%$ . Figure 7 depicts the comparison between the uncontrolled solution (i. e.  $\gamma(t) = 0$ ) of the reduced model and the projection of the finite volume solution for reduced models computed with a reference control  $\gamma_{ref} = 0$  and  $\gamma_{ref} = \gamma_{chirp}$ , respectively.

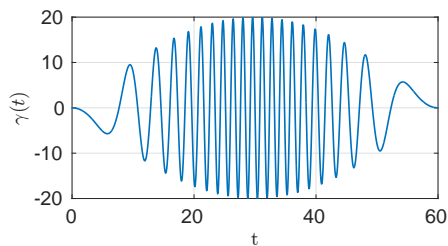


**Figure 6:** Chirping function used for the computation of the snapshot matrix.

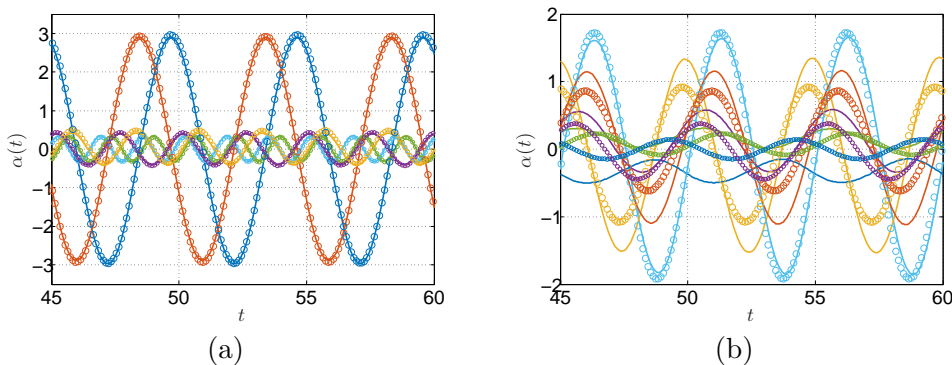


**Figure 7:** First six modes of (6), (7) (—) and projection of FEM solution (o) for two reduced order models with different reference controls. (a)  $\gamma_{ref} = 0$ . (b)  $\gamma_{ref} = \gamma_{chirp}$ .

Figure 8 shows the first four POD modes for the uncontrolled solution. The modes occur in pairs, the second one slightly shifted downstream. This is due to symmetries in the problem. The first four modes already account for  $\approx 98\%$  of the information, cf. Figure 9, where in (a) the eigenvalues are shown for both the uncontrolled flow and the flow controlled by the chirping function. The error, i. e. the ratio of the truncated eigenvalues, is visualized in (b).

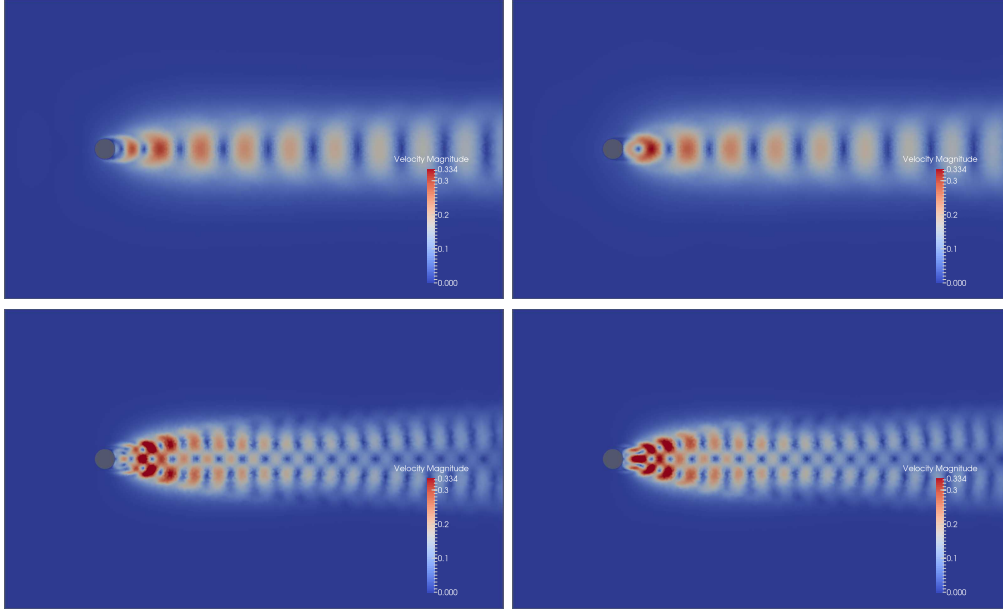


**Figure 8:** The first four POD modes for an uncontrolled solution.

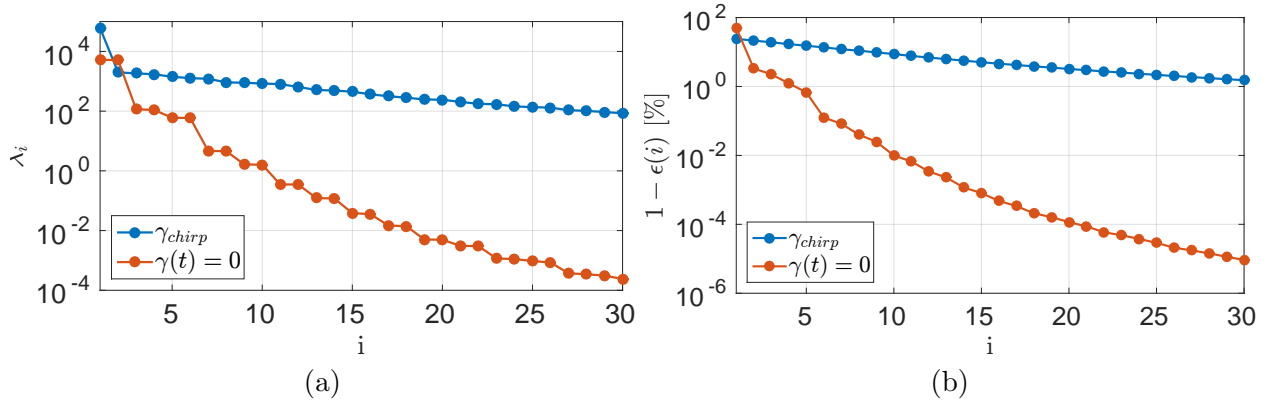


**Figure 9:** Eigenvalues (a) and error at current basis size (b) for an uncontrolled solution and a solution controlled by the chirping function.

---

#### 4.4 Adjoint systems

The first step for the application of the reference point method (Section 3.1.1) is to transform (R-MOCP) into a sequence of single objective optimization problems:

$$\begin{aligned} \min_{\alpha, \gamma} \bar{J}(\alpha, \gamma) &= \min_{\alpha, \gamma} \|T - J(\alpha, \gamma)\|_2^2, & (\text{SOP}) \\ \text{with } \bar{J}(\alpha, \gamma) &= (T_1 - J_1(\alpha, \gamma))^2 + (T_2 - J_2(\alpha, \gamma))^2 \\ &= \left( T_1 - \int_{t_0}^{t_e} \sum_{i=1}^l \alpha_i^2(t) dt \right)^2 + \left( T_2 - l \int_{t_0}^{t_e} \gamma^2(t) dt \right)^2, & (10) \end{aligned}$$

where  $\alpha(t)$  fulfills the reduced order state equation (6), (7).

The task is now to solve a sequence of scalar optimization problems with varying targets  $T$ . The problem (SOP) is solved by a backtracking method [NW06]. For this purpose, the necessary gradient information is computed with an adjoint approach. We therefore introduce the adjoint state  $\lambda \in H^1([t_0, t_e], \mathbb{R}^l)$  and the Lagrange functional:

$$L(\alpha, \lambda, \gamma) = \bar{J}(\alpha, \gamma) - \int_{t_0}^{t_e} \lambda^T (\dot{\alpha} - \mathcal{A} - \mathcal{B}\alpha - \mathcal{C}(\alpha) - \mathcal{D}\dot{\gamma} - (\mathcal{E} + \mathcal{F}\alpha)\gamma - \mathcal{G}\gamma^2) dt, \quad (11)$$

which is stationary for optimal values of  $\alpha(t)$  and  $\gamma(t)$ :

$$\delta L(\delta\alpha, \delta\lambda, \delta\gamma) = \left( \frac{\partial L}{\partial \alpha}, \delta\alpha \right)_{L^2} + \left( \frac{\partial L}{\partial \lambda}, \delta\lambda \right)_{L^2} + \left( \frac{\partial L}{\partial \gamma}, \delta\gamma \right)_{L^2} = 0. \quad (12)$$

Using integration by parts, this leads to the following system of equations<sup>1</sup>:

$$\dot{\alpha} = \mathcal{A} + \mathcal{B}\alpha + \mathcal{C}(\alpha) + \mathcal{D}\dot{\gamma} + (\mathcal{E} + \mathcal{F}\alpha)\gamma + \mathcal{G}\gamma^2, \quad (13)$$

$$\dot{\lambda} = -\frac{\partial \bar{J}}{\partial \alpha} - \left( \mathcal{B} + \frac{\partial \mathcal{C}(\alpha)}{\partial \alpha} + \mathcal{F}\gamma \right)^T \lambda, \quad (14)$$

$$0 = \frac{\partial \bar{J}}{\partial \gamma} + (\mathcal{E} + \mathcal{F}\alpha + 2\mathcal{G}\gamma)^T \lambda - \mathcal{D}^T \dot{\lambda}, \quad (15)$$

with the Fréchet derivatives:

$$\begin{aligned} \partial \bar{J} / \partial \alpha_j &= 4 \left( \int_{t_0}^{t_e} \sum_{i=1}^l \alpha_i^2(t) dt - T_1 \right) \alpha_j(t), \\ \partial \bar{J} / \partial \gamma &= 4l \left( l \int_{t_0}^{t_e} \gamma^2(t) dt - T_2 \right) \gamma(t), \end{aligned}$$

and the respective boundary conditions  $\alpha(0) = \alpha_0$  and  $\lambda(t_e) = 0$ . Equations (13) – (15) form the so-called optimality system which is seldom solved explicitly. Instead, the state equation (13) and the adjoint equation (14) are solved by forward and backward integration, respectively. The optimality condition (15) provides the derivative information of the cost functional with respect

---

**Algorithm 3** (Adjoint based scalar optimization)

---

**Require:** Target point  $T$ , initial guess  $\gamma^0$

- 1: **for**  $i = 0, \dots$  **do**
  - 2:     Compute  $\alpha^i$  by solving the reduced order model (13) with the control  $\gamma^i$
  - 3:     Solve the adjoint equation (14) in backwards time with  $\gamma^i, \alpha^i, \partial\bar{J}/\partial\alpha^i$
  - 4:     Compute the gradient  $D_\gamma\bar{J}^i$  by evaluating the optimality condition (15) with  $\gamma^i, \alpha^i$  and  $\lambda^i$
  - 5:     Update the control:  $\gamma^{i+1} = \gamma^i + a^i d^i$ , where  $a^i$  is the step length computed by the backtracking Armijo method [NW06] and  $d^i$  is the conjugate gradient direction  $d^i = -D_\gamma\bar{J}^i + \beta^i d^{i-1}$ ,  
 $d^0 = D_\gamma\bar{J}^0$  with  $\beta^i = \frac{D_\gamma\bar{J}^i \cdot D_\gamma\bar{J}^i}{D_\gamma\bar{J}^{i-1} \cdot D_\gamma\bar{J}^{i-1}}$
  - 6: **end for**
- 

to the control  $\gamma$ . This information can be used to improve an initial guess for the optimal control within an iterative optimization scheme as described in Algorithm 3.

In [BCB05], the condition  $\lambda(t_e) = 0$  is the only boundary condition of the adjoint equation. However, in the exact derivation, the equation  $\lambda^T(t_0)\mathcal{D}\delta\gamma(t_0) = 0$  also has to be satisfied which is neglected. In our computations, this caused convergence issues which is why we now derive a second optimality system based on an alternative formulation of the reduced model. Following [Rav99], we define an augmented state  $z = (\alpha, \gamma)^T$  and introduce a new control  $v \in L^2([t_0, t_e], \mathbb{R})$ ,  $v(t) = \dot{\gamma}(t)$ . It is known from optimal control theory that if a dynamical system depends linearly on the control, the control is bounded by box constraints (as it is for physical reasons) and the control does not appear in the cost functional, as is now the case, the optimal control is of *bang bang* type and might include singular arcs [Ger12]. Since the computation of such solutions is numerically challenging, we avoid this behavior by adding a regularization term to the second objective in (R-MOCP), i. e.  $J_2 = l\|\gamma\|_{L^2}^2 + \beta\|v\|_{L^2}^2$ , where  $\beta$  is a small number (here:  $\beta = 1e^{-5}$ ). The optimality system can be derived in an analogous way to the one described above, where the adjoint states are now denoted by  $\lambda \in H^1([t_0, t_e], \mathbb{R}^l)$  and  $\mu \in H^1([t_0, t_e], \mathbb{R})$ :

$$\dot{\alpha} = \mathcal{A} + \mathcal{B}\alpha + \mathcal{C}(\alpha) + \mathcal{D}v + (\mathcal{E} + \mathcal{F}\alpha)\gamma + \mathcal{G}\gamma^2, \quad (16)$$

$$\dot{\gamma} = v, \quad (17)$$

$$\dot{\lambda} = -\frac{\partial\bar{J}}{\partial\alpha} - \left(\mathcal{B} + \frac{\partial\mathcal{C}(\alpha)}{\partial\alpha} + \mathcal{F}\gamma\right)^T \lambda, \quad (18)$$

$$\dot{\mu} = -\frac{\partial\bar{J}}{\partial\gamma} - (\mathcal{E} + \mathcal{F}\alpha + 2\mathcal{G}\gamma)^T \lambda, \quad (19)$$

$$0 = \frac{\partial\bar{J}}{\partial v} + \mathcal{D}^T \lambda + \mu, \quad (20)$$

---

<sup>1</sup>Note, that since this approach makes use of variational calculus, it is formally only applicable in the case of stronger assumptions, namely for  $\alpha, \lambda, \gamma \in C^1$  (since we apply integration by parts).



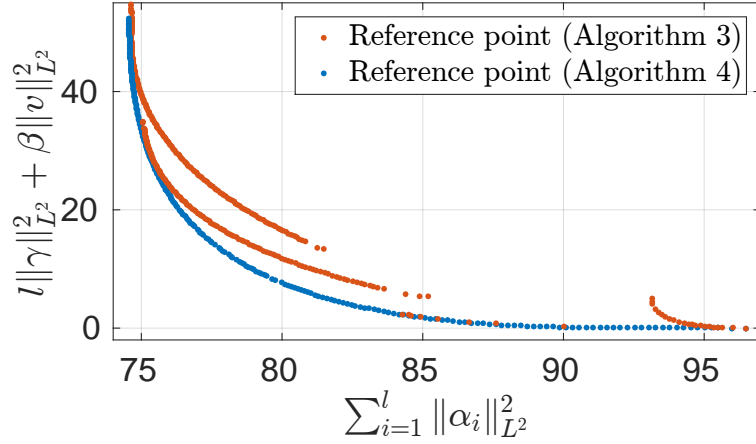


**Figure 10:** Comparison of the Pareto fronts computed with the two optimality systems (13) – (15) and (16) – (20).

with the Fréchet derivatives:

$$\begin{aligned}\partial\bar{J}/\partial\gamma &= 4l \left( l \int_{t_0}^{t_e} \gamma^2(t) dt + \beta \int_{t_0}^{t_e} v^2(t) dt - T_2 \right) \gamma(t), \\ \partial\bar{J}/\partial v &= 4\beta \left( l \int_{t_0}^{t_e} \gamma^2(t) dt + \beta \int_{t_0}^{t_e} v^2(t) dt - T_2 \right) v(t),\end{aligned}$$

$\partial\bar{J}/\partial\alpha_j$  as before and the respective boundary conditions

$$\alpha(0) = \alpha_0, \quad \lambda(T) = 0, \quad \mu(0) = 0, \quad \mu(T) = 0. \quad (21)$$

This yields a boundary value problem for the state equations (16), (17) and the adjoint equations (18), (19) which can, for a given control  $v$ , be solved by an iterative scheme. Applying a shooting method, the initial value  $\gamma(0)$  is computed such that  $\mu(0) = 0$  is satisfied using Newton’s method (cf. Algorithm 4). This is computationally more expensive than the simple forward-backward integration in Algorithm 3. However, the system (16) – (20) yields strongly improved convergence and decreased sensitivity to the optimization parameters in comparison to the system (13) – (15). This is depicted in Figure 10, where the Pareto front based on (16) – (20) was computed executing Algorithm 4 once, starting in the already known point of zero control cost. In contrast to that, several attempts were made with Algorithm 3, starting from different points on the Pareto front. All of them either divert quickly from the front or stop prematurely. All the results shown in Section 5 are therefore based on (16) – (20).

## 5 Results

In this section we present solutions to (R-MOCP) obtained with the algorithms presented in Sections 3.1 and 4.4. For all cases, we fix the time interval  $[t_0, t_e]$  to  $[0, 10]$ , which corresponds to

---

**Algorithm 4** (Adjoint based scalar optimization with shooting)

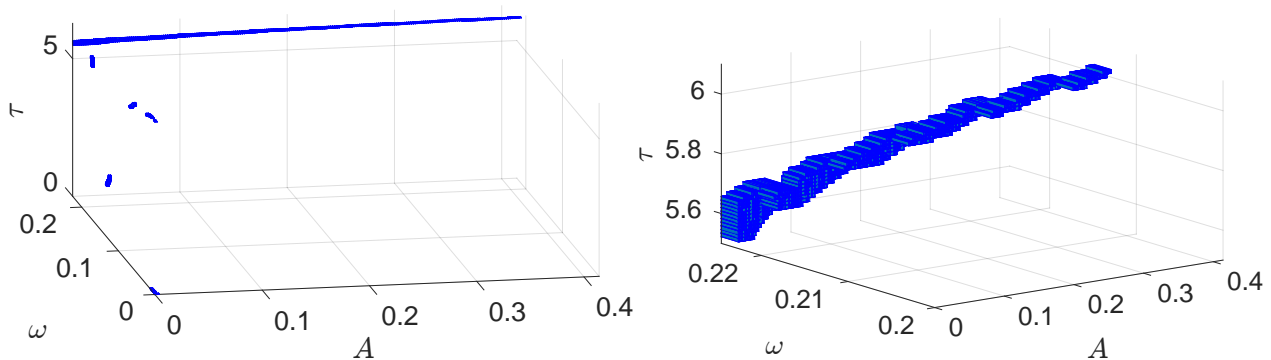
---

**Require:** Target point  $T$ , initial guess  $v^0$

- 1: **for**  $i = 0, \dots$  **do**
  - 2:   Shooting step: Determine  $\gamma^i(0)$  by solving an internal root finding problem in order to enforce the condition  $\mu^i(0) = 0$ ; This step requires forward solves of (16), (17) and backward solves of (18), (19)
  - 3:   Compute  $(\alpha^i, \gamma^i)$  by solving the reduced order model (16), (17) with  $v^i$  as the control and  $\gamma^i(0)$
  - 4:   Solve the adjoint equations (18), (19) in backwards time with  $v^i$ ,  $(\alpha^i, \gamma^i)$ ,  $\partial\bar{J}/\partial\alpha^i$  and  $\partial\bar{J}/\partial\gamma^i$
  - 5:   Compute the gradient  $D_v\bar{J}^i$  by evaluating the optimality condition (20) with  $\lambda^i$  and  $\mu^i$ .
  - 6:   Update the control:  $v^{i+1} = v^i + a^i d^i$ , with  $a^i$  and  $d^i$  as in Algorithm 3
  - 7: **end for**
- 

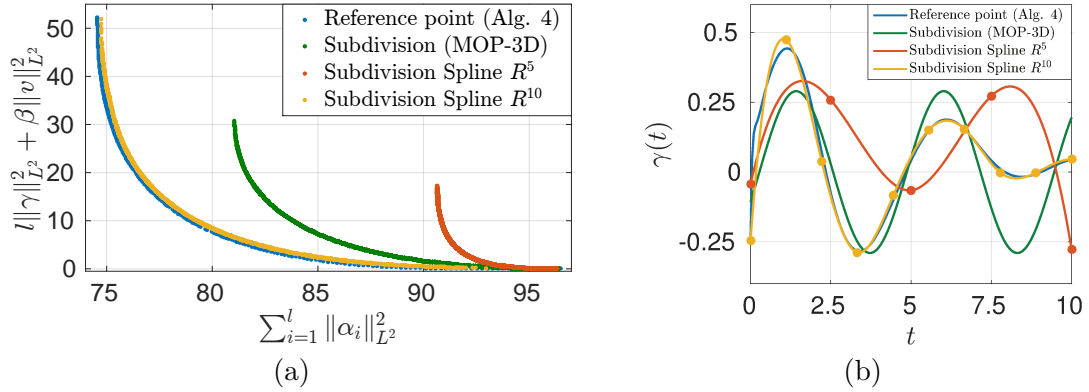
roughly two vortex shedding cycles. In order to use the subdivision method, we define an embedding  $E : \mathbb{R}^s \rightarrow L^2([t_0, t_e], \mathbb{R})$  transforming (MOCP) into a multiobjective optimization problem with moderate decision space dimension ( $s \leq 10$ ). One way to do this is by assuming a sinusoidal control (cf. Section 3.1.2) which then yields (MOP-3D). Another way is to interpret the sampling points  $p \in \mathbb{R}^s$  as coefficients of a cubic spline with  $s$  breakpoints. For the reference point method, we discretize  $\gamma$  with a constant step length of  $\Delta t = 0.05$  and solve Equations (16) – (19) with a fourth order Runge-Kutta scheme.

Figure 11 shows the box covering of the Pareto set for (MOP-3D), the respective Pareto front is shown in Figure 12. It is noteworthy that, apart from a few spurious points at  $A \approx 0$  caused by numerical errors (Figure 5(a)), the largest part of the set is restricted to a small part of the frequency domain. This is comprehensible since the rotation counteracts the natural dynamics of the von Kármán vortex street. The trade-off between control cost and stabilization is almost exclusively realized by changing the amplitude of the rotation. When moving towards the two



**Figure 11:** Solution of (MOP-3D) with global subdivision algorithm after 27 subdivision steps.

scalar optimal solutions, i. e. minimal fluctuations and minimal control cost, respectively, further



**Figure 12:** (a) Comparison of Pareto fronts for different MOCP solution methods. (b) Comparison of the Pareto optimal controls with equal cost ( $J_2 = 15$ ) for different MOCP solution methods.

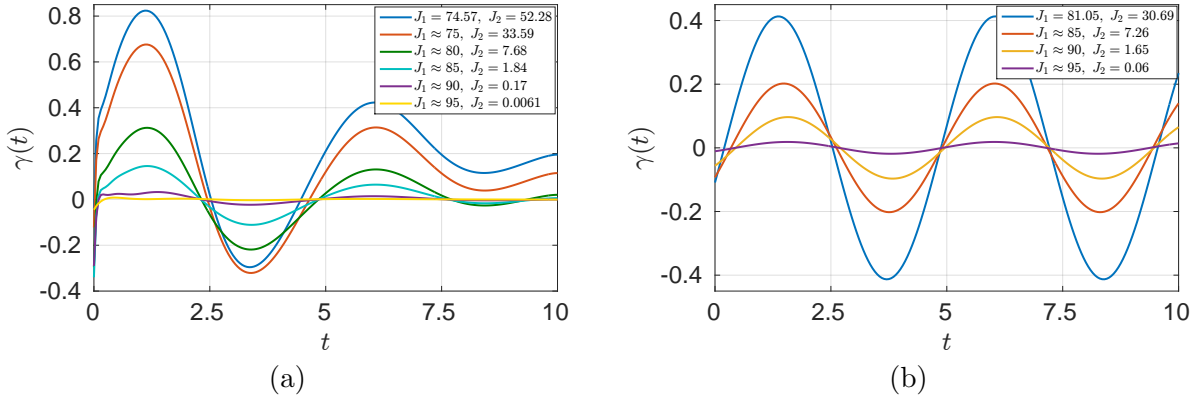


**Figure 13:** Different Pareto points for the Reference point method (a) and (MOP-3D) (b).

improvements are only possible by accepting large trade-offs in the other objective which is a common phenomenon in multiobjective optimization. When designing a system, one could now accept a small increase in the main objective, i. e. flow stabilization, in order to achieve a large decrease in the control cost. This becomes more clear when looking at Figure 13(b), where different optimal compromises for the control are shown. For a relatively small improvement of  $J_1$  from 85 to 81.05 ( $\approx -5\%$ ), the control cost increase by 322%.

Figures 12(a) and 13 also show the Pareto fronts and Pareto optimal controls, respectively, computed with the other methods, i. e. two different spline approximations ( $s = 5$  and  $s = 10$ ) computed with the subdivision algorithm on the one hand and arbitrary control functions determined by the reference point method on the other hand. We observe that a spline with 5 breakpoints is too restrictive to find control functions of acceptable quality. When using 10 breakpoints on the other hand, the Pareto front clearly surpasses the solution of (MOP-3D). It is, however, numerically expensive to compute. The best solution is computed with the reference point method. The im-

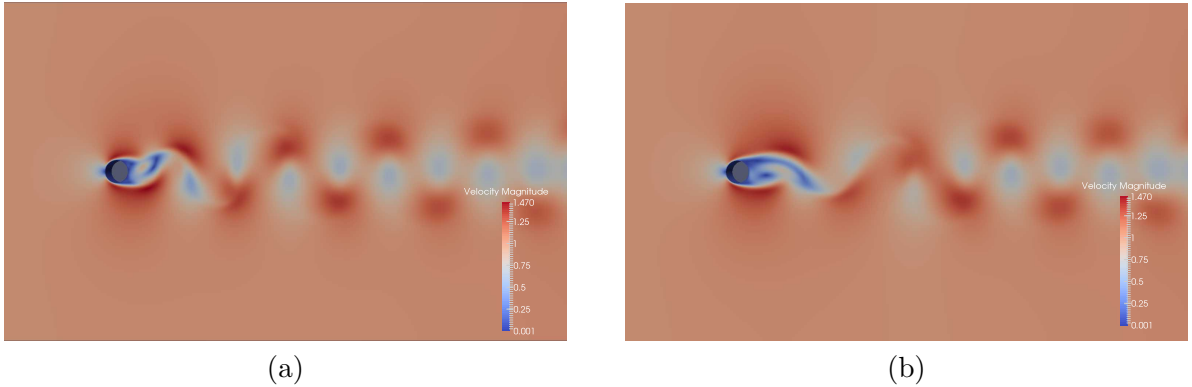


**Figure 14:** FV solution at  $t_e = 10$  with two different controls computed with the Reference point method. (a)  $J_2 = 85$ . (b)  $J_2 = 75$

**Table 1:** Comparison of CPU time of different methods (Subdivision algorithm in parallel: CPU time = Number of CPUs times wall clock time).

	# boxes / points	# Function evaluations	# Adjoint evaluations	CPU time [h]
Subdivision (MOP-3D)	1383	$\approx 8.3 \cdot 10^6$	0	$\approx 1132$
Subdivision Spline $\mathbb{R}^5$	6057	$\approx 11.1 \cdot 10^6$	0	$\approx 1512$
Subdivision Spline $\mathbb{R}^{10}$	1880	$\approx 42 \cdot 10^6$	0	$\approx 5875$
Reference point (16) – (20)	256	26781	1002	$\approx 12.2$

provement over the spline-based solution is relatively low, the reason being that the controls are almost similar (see Figure 12(b) where solutions of the different methods with the same control cost  $J_2 = 15$  are compared). When considering scenarios with larger time intervals than 10 seconds, the spline dimension would have to be increased further leading to again much higher computational cost whereas the cost for the reference point method increase only linearly with time due to the fact that only the number of time steps in the forward and backward integration (16) – (19) is affected. Finally, Figure 14 shows two solutions of (1a) – (1f) with controls computed by the reference point method, corresponding to different control cost  $J_2$  and hence different degrees of stabilization. Due to the relatively short integration time of  $t_e = 10$  seconds, changes are only apparent closely past the cylinder. Still, we observe increased stabilization when allowing higher control cost.

From a computational point of view, the reference point method has the clear advantage, cf. Table 5. This is not surprising since, in order to have a good representation of a box, a large number of sample points needs to be evaluated. This is already numerically expensive in 3D and more so for a spline-based embedding, i. e. we need to pay a price for global optimality and the derivative free approach. For future work, it is therefore advisable to utilize the gradient based version of the subdivision algorithm in order to decrease the computational cost.

---

## 6 Conclusion

In this article, we present different approaches for numerically solving multiobjective optimal control problems involving boundary control of the Navier-Stokes equations. To the best of our knowledge, this is the first article where multiobjective optimal control is applied in the context of nonlinear PDEs. In order to reduce the computational effort, model order reduction via proper orthogonal decomposition and Galerkin projection is used to compute a controllable reduced model of ODEs. Different multiobjective optimal control algorithms are introduced and their respective advantages and disadvantages are discussed. The subdivision algorithm yields a box covering of globally optimal Pareto sets and can also deal with problems where the set is disconnected. Since its applicability depends critically on both the decision space dimension and the numerical effort of function evaluations, it is restricted to moderate decision space dimensions. To solve optimal control problems, the control function therefore has to be represented by a low number of parameters, e. g. by a harmonic function or spline coefficients. The reference point method converts the multiobjective optimal control problem into a sequence of scalar optimal control problems that can be solved using well known procedures from single objective optimal control theory, also for high decision space dimensions. To incorporate gradient information, the optimality system is derived for the scalar problem. In combination with good initial guesses from the previous scalar problem, the Pareto set can be approximated very efficiently. The method is of local nature, however, such that the initial guesses for the scalar problems as well as the selection of the first target point is important. Additionally, the selection of target points becomes tedious for higher objective space dimensions. The computed Pareto set yields considerably more information about the system than the solution of a single objective optimization. A decision maker can use this information to make well-founded decisions on how to control the system or even to devise adaptive control strategies reacting to changing priorities, e. g. the need to save energy.

There are numerous applications where multiobjective optimal control for systems described by PDEs is of great interest, e. g. minimizing the drag and maximizing the lift of airplanes, minimizing the weight and maximizing the stability of structures, optimal mixing with minimal cost, control of flow patterns and vortices in HVAC applications, to name a few. A question that needs to be addressed in the future is the error control for the reduced model in order to guarantee optimality for the PDE based problem. Several authors have addressed this for scalar optimization with reduced order models [Fah00, KV02, VP05, BCB07, GV13, Las14] and additional questions arise in the context of multiobjective optimal control.

**Acknowledgement:** This research was partially funded by the German Federal Ministry of Education and Research (BMBF) within the Leading-Edge Cluster "Intelligent Technical Systems OstWestfalenLippe" (its OWL). Calculations leading to the results presented here were performed on resources provided by the Paderborn Center for Parallel Computing (PC<sup>2</sup>).

## References

- [AJG05] A. Abraham, L. Jain, and R. Goldberg, editors. *Evolutionary multiobjective optimization*. Springer London, 2005.

- 
- [ASG01] A. C. Antoulas, D. C. Sorensen, and S. Gugercin. A survey of model reduction methods for large-scale systems. *Contemporary mathematics*, 280:193–220, 2001.
- [BBI09] M. Bergmann, C. H. Bruneau, and A. Iollo. Enablers for robust POD models. *Journal of Computational Physics*, 228(2):516–538, 2009.
- [BCB05] M. Bergmann, L. Cordier, and J.-P. Brancher. Optimal rotary control of the cylinder wake using proper orthogonal decomposition reduced-order model. *Physics of Fluids*, 17(9):097101, 2005.
- [BCB07] M. Bergmann, L. Cordier, and J.-P. Brancher. Drag minimization of the cylinder wake by trust-region proper orthogonal decomposition. *Notes on Numerical Fluid Mechanics and Multidisciplinary Design*, 95:309–324, 2007.
- [BHL93] G. Berkooz, P. Holmes, and J. L. Lumley. The proper orthogonal decomposition in the analysis of turbulent flows. *Annual Review of Fluid Mechanics*, 25(1971):539–575, 1993.
- [BMNP04] M. Barrault, Y. Maday, N. C. Nguyen, and A. T. Patera. An empirical interpolation method: application to efficient reduced-basis discretization of partial differential equations. *Comptes Rendus Mathematique*, 339(9):667–672, November 2004.
- [BMS05] P. Benner, V. Mehrmann, and D. C. Sorensen, editors. *Dimension Reduction of Large-Scale Systems*. Springer Berlin Heidelberg New York, 2005.
- [CBS05] M. Couplet, C. Basdevant, and P. Sagaut. Calibrated reduced-order POD-Galerkin system for fluid flow modelling. *Journal of Computational Physics*, 207:192–220, 2005.
- [CEF09] L. Cordier, B. A. El Majd, and J. Favier. Calibration of POD reduced-order models using Tikhonov regularization. *International Journal for Numerical Methods in Fluids*, 63(2):269–296, 2009.
- [Deb99] K. Deb. Multi-objective Genetic Algorithms: Problem Difficulties and Construction of Test Problems. *Evolutionary computation*, 7(3):205–30, January 1999.
- [DEF<sup>+</sup>14] M. Dellnitz, J. Eckstein, K. Flaßkamp, P. Friedel, C. Horenkamp, U. Köhler, S. Ober-Blöbaum, S. Peitz, and S. Tiemeyer. Multiobjective Optimal Control Methods for the Development of an Intelligent Cruise Control. In *ECMI 2014 Proceedings*, Taormina, Italy, 2014.
- [DH97] M. Dellnitz and A. Hohmann. A subdivision algorithm for the computation of unstable manifolds and global attractors. *Numerische Mathematik*, 75(3):293–317, 1997.
- [DSH05] M. Dellnitz, O. Schütze, and T. Hestermeyer. Covering Pareto Sets by Multilevel Subdivision Techniques. *Journal of Optimization Theory and Applications*, 124(1):113–136, January 2005.
-

- 
- [Ehr05] M. Ehrgott. *Multicriteria optimization*. Springer Berlin Heidelberg New York, 2nd editio edition, 2005.
- [Fah00] M. Fahl. *Trust-Region Methods for Flow Control Based on Reduced Order Modelling*. Phd thesis, University of Trier, 2000.
- [FGH98] A. V. Fursikov, M. D. Gunzburger, and L. S. Hou. Boundary value problems and optimal boundary control for the navier-stokes system: the two-dimensional case. *SIAM Journal on Control and Optimization*, 36(3):852–894, 1998.
- [FP12] J. H. Ferziger and M. Peric. *Computational methods for fluid dynamics*. Springer Science & Business Media, 2012.
- [GBZI04] B. Galletti, C. H. Bruneau, L. Zannetti, and A. Iollo. Low-order modelling of laminar flow regimes past a confined square cylinder. *Journal of Fluid Mechanics*, 503(July):161–170, 2004.
- [GeH89] M. Gad-el Hak. Flow control. *Applied mechanics reviews*, 42(10):261–293, 1989.
- [Ger12] M. Gerds. *Optimal control of ODEs and DAEs*. Walter de Gruyter, 2012.
- [GMNP07] M. A. Grepl, Y. Maday, N. C. Nguyen, and A. T. Patera. Efficient Reduced-Basis Treatment of Nonaffine and Nonlinear Partial Differential Equations. *ESAIM: Mathematical Modelling and Numerical Analysis*, 41(3):575–605, 2007.
- [GPT99] W. R. Graham, J. Peraire, and K. Y. Tang. Optimal control of vortex shedding using low-order models - Part I: Open-Loop Model Development. *International Journal for Numerical Methods in Engineering*, 44(7):945–972, 1999.
- [GV13] M. Gubisch and S. Volkwein. Proper Orthogonal Decomposition for Linear-Quadratic Optimal Control. *Bibliothek der Universität Konstanz*, 2013.
- [Hil01] C. Hillermeier. *Nonlinear Multiobjective Optimization: A Generalized Homotopy Approach*. Birkhäuser, 2001.
- [HLB98] P. Holmes, J. L. Lumley, and G. Berkooz. *Turbulence, coherent structures, dynamical systems and symmetry*. Cambridge university press, 1998.
- [HPUU08] M. Hinze, R. Pinnau, M. Ulbrich, and S. Ulbrich. *Optimization with PDE constraints*. Springer Science+Business Media, 2008.
- [HRT96] J. G. Heywood, R. Rannacher, and S. Turek. Artificial Boudaries and Flux and Pressure Conditions for the Incompressible Navier-Stokes Equations. *International Journal for Numerical Methods in Fluids*, 22(5):325–352, March 1996.
- [IR01] K. Ito and S. S. Ravindran. Reduced Basis Method for Optimal Control of Unsteady Viscous Flows. *International Journal of Computational Fluid Dynamics*, 15(2):97–113, October 2001.

- 
- [JJT07] H. Jasak, A. Jemcov, and Z. Tukovic. OpenFOAM : A C ++ Library for Complex Physics Simulations. *International Workshop on Coupled Methods in Numerical Dynamics*, m:1–20, 2007.
- [KV02] K. Kunisch and S. Volkwein. Galerkin Proper Orthogonal Decomposition Methods for a General Equation in Fluid Dynamics. *SIAM Journal on Numerical Analysis*, 40(2):492–515, January 2002.
- [Lac14] G. V. Lachmann. *Boundary layer and flow control: its principles and application*. Elsevier, 2014.
- [Las14] O. Lass. *Reduced order modeling and parameter identification for coupled nonlinear PDE systems*. PhD thesis, University of Konstanz, 2014.
- [LHDVI10] F. Logist, B. Houska, M. Diehl, and J. Van Impe. Fast pareto set generation for nonlinear optimal control problems with multiple objectives. *Structural and Multidisciplinary Optimization*, 42:591–603, 2010. 10.1007/s00158-010-0506-x.
- [LKBM05] A. V. Lotov, G. K. Kamenev, V. E. Berezkin, and K. Miettinen. Optimal control of cooling process in continuous casting of steel using a visualization-based multi-criteria approach. *Applied Mathematical Modelling*, 29:653–672, 2005.
- [LMW12] A. Logg, K.-A. Mardal, and G. N. Wells, editors. *Automated Solution of Differential Equations by the Finite Element Method: The FEniCS book*. Springer Science & Business Media, 84 edition, 2012.
- [Lum67] J. L. Lumley. The structure of inhomogeneous turbulent flows. *Atmospheric turbulence and radio wave propagation*, pages 166–178, 1967.
- [Mie99] K. Miettinen. *Nonlinear Multiobjective Optimization*. Kluwer Academic Publishers, 1999.
- [NPM05] B. R. Noack, P. Papas, and P. A. Monkewitz. The need for a pressure-term representation in empirical Galerkin models of incompressible shear flows. *Journal of Fluid Mechanics*, 523:339–365, 2005.
- [NW06] J. Nocedal and S. J. Wright. *Numerical Optimization*. Springer Science & Business Media, 2006.
- [OBPG15] S. Ober-Blöbaum and K. Padberg-Gehle. Multiobjective optimal control of fluid mixing. In *Proceedings in Applied Mathematics and Mechanics (PAMM)*, 2015.
- [OBRzF12] S. Ober-Blöbaum, M. Ringkamp, and G. zum Felde. Solving multiobjective optimal control problems in space mission design using discrete mechanics and reference point techniques. In *51st IEEE International Conference on Decision and Control*, pages 5711–5716, Maui, HI, USA, 10-13 December 2012.



- 
- [PD15] S. Peitz and M. Dellnitz. Multiobjective Optimization of the Flow Around a Cylinder Using Model Order Reduction. In *Proceedings in Applied Mathematics and Mechanics (PAMM)*, 2015.
- [Rav99] S. S. Ravindran. *Proper orthogonal decomposition in optimal control of fluids*, volume 99. National Aeronautics and Space Administration, Langley Research Center, 1999.
- [RBW<sup>+</sup>09] C. Romaus, J. Böcker, K. Witting, A. Seifried, and O. Znamenshchykov. Optimal energy management for a hybrid energy storage system combining batteries and double layer capacitors. In *Energy Conversion Congress and Exposition, 2009. ECCE 2009. IEEE*, pages 1640–1647, San Jose, CA, USA, 2009. IEEE Xplore Digital Library, Los Alamitos.
- [Rem00] D. Rempfer. On Low-Dimensional Galerkin Models for Fluid Flow. *Theoretical and Computational Fluid Dynamics*, 14(2):75–88, 2000.
- [Row05] C. W. Rowley. Model Reduction for Fluids, Using Balanced Proper Orthogonal Decomposition. *International Journal of Bifurcation and Chaos*, 15(03):997–1013, March 2005.
- [Sir87] L. Sirovich. Turbulence and the dynamics of coherent structures Part I: coherent structures. *Quarterly of Applied Mathematics*, XLV(3):561–571, 1987.
- [SK04] S. Sirisup and G. E. Karniadakis. A spectral viscosity method for correcting the long-term behavior of POD models. *Journal of Computational Physics*, 194(1):92–116, 2004.
- [SvdVR05] W. Schilders, H. A. van der Vorst, and J. Rommes, editors. *Model Order Reduction*. Springer Berlin Heidelberg, 2005.
- [SWOBD13] O. Schütze, K. Witting, S. Ober-Blöbaum, and M. Dellnitz. Set Oriented Methods for the Numerical Treatment of Multiobjective Optimization Problems. In E. Tantar, A.-A. Tantar, P. Bouvry, P. Del Moral, P. Legrand, C. A. Coello Coello, and O. Schütze, editors, *EVOLVE- A Bridge between Probability, Set Oriented Numerics and Evolutionary Computation*, volume 447 of *Studies in Computational Intelligence*, pages 187–219. Springer Berlin Heidelberg, 2013.
- [VP05] K. Veroy and A. T. Patera. Certified real-time solution of the parametrized steady incompressible Navier-Stokes equations: Rigorous reduced-basis a posteriori error bounds. *International Journal for Numerical Methods in Fluids*, 47(April 2004):773–788, 2005.
- [WP02] K. Willcox and J. Peraire. Balanced Model Reduction via the Proper Orthogonal Decomposition. *AIAA Journal*, 40(11):2323–2330, November 2002.

- 
- [XFB<sup>+</sup>14] D. Xiao, F. Fang, A.G. Buchan, C.C. Pain, I.M. Navon, J. Du, and G. Hu. Non-linear model reduction for the NavierStokes equations using residual DEIM method. *Journal of Computational Physics*, 263:1–18, 2014.
- [ZDT00] E. Zitzler, K. Deb, and L. Thiele. Comparison of multiobjective evolutionary algorithms: empirical results. *Evolutionary computation*, 8(2):173–95, January 2000.